# Supplementary material

### S1 Eruptions considered

## Askja 1875

Askja, within Iceland's Northern Volcanic Zone (NVZ), erupted in six phases of varying intensity, lasting 17 hours on 28–29 March 1875. The main eruption included a Subplinian phase (Unit B) followed by hydromagmatic fall and with some proximal pyroclastic flow (Unit C) and a magmatic Plinian phase (Unit D). Units C and D consisted of $4.5 \times 10^8$ $m^3$ and $1.37 \times 10^9$ $m^3$ of rhyolitic tephra, respectively [1–3].

## Eyjafjallajökull 2010

Eyjafjallajökull is situated in the Eastern Volcanic Zone (EVZ) in southern Iceland. The Subplinian 2010 eruption lasted from 14 April to 21 May, resulting in significant disruption to European airspace. Plume heights ranged from 3 to 10 km and dispersing $2.7 \times 10^5$ $m^3$ of trachytic tephra [4].

## Hverfjall 2000 BP

Hverfjall Fires occurred from a 50 km long fissure in the Krafla Volcanic System in Iceland's NVZ. Magma interaction with an aquifer resulted in an initial basaltic hydromagmatic fall deposit from the Hverfjall vent with a total volume of $8 \times 10^7$ $m^3$ [5].

## Eldgja 10th century

The flood lava eruption in the first half of the $10^{th}$ century occurred from the Eldgja fissure within the Katla Volcanic System in Iceland's EVZ. The mainly effusive basaltic eruption is estimated to have lasted between 6 months and 6 years, and included approximately 16 explosive episodes, both magmatic and hydromagmatic. A subaerial eruption produced magmatic Unit 7 ($2.4 \times 10^7$ $m^3$ of tephra) and a subglacial eruption produced hydromagmatic Unit 8 ($2.8 \times 10^7$ $m^3$ of tephra). Plume heights for both phases are estimated at 11–18 km [6].

## Grímsvötn 2004 and 2011

Grímsvötn lies beneath the Vatnajökull ice cap in Iceland's EVZ. The 1–6 November 2004 eruption started beneath ~ 200 m thick ice, and magma took approximately 30 minutes to reach the surface. Hydromagmatic Unit A, consisting of $5 \times 10^5$ $m^3$ of tachylitic tephra with low vesicularity, was dispersed to the north from a 6 km high plume during the initial subaerial phase. Units B to G consisted of pyroclastic density currents (PDCs), some combined with fall deposits [7].

The May 21–28, 2011 eruption was the most explosive at Grímsvötn for over a century [8], with a 15–20 km high plume dispersing 6–8 x $10^8$ $m^3$ of basaltic tephra. High wind shear resulted in low-level dispersal to the south (< 4 km altitude) and northerly dispersal at higher altitudes. Alternating water-rich and water-poor phases produced units consisting of fine ash with accretionary lapilli (hydromagmatic) and pumice-rich lapilli (magmatic) [9].

## Hekla

Hekla is located on the western edge of Iceland's EVZ and has experienced 18 explosive eruptions since 870 CE. High-intensity eruptions in 1104 and 1300 produced columns 20–25 km high. The 1104 dacitic eruption dispersed 1.2 x $10^9$ $m^3$ tephra to the north and in 1300, 1 x $10^8$ $m^3$ andesitic tephra was dispersed to the northeast. Subplinian eruptions in 1693 in 1766 each deposited ~ 2 x $10^8$ $m^3$ of andesitic tephra towards the north from plumes up to 18 km high [10, 11].

An hour-long Plinian eruption on 2 September 1845 deposited 1.3 x $10^8$ $m^3$ of andesitic tephra east–southeast from a 19 km plume [12]. On 17 January 1991, a 50 minute long explosive eruption dispersed 1.6–1.9 x $10^8$ $m^3$ of basaltic-andesite tephra from a plume blown north–northeast in strong winds and reaching 10.3–12.7 km above sea level [13]. On 26 February 2000, a Subplinian eruption lasting approximately 30 minutes dispersed ~ 1 x $10^6$ $m^3$ basaltic-andesite tephra to the north from a plume 12 km high [14].

## Jan Mayen 1732

Beerenberg Volcano on Jan Mayen Island is situated at the northern end of the mid-Atlantic Ridge and is the northernmost active subaerial volcano. The 1732 Surtseyan eruption on the southwestern flank lasted 4–40 days from historic accounts. A plume of 9–12 km deposited a total volume of ~ 4 × $10^8$ $m^3$ basanitic tephra [15].

## Reykjanes 1226

The vent for the 1226 eruption in the Reykjanes Volcanic Belt, southwest Iceland, is estimated to have been ~ 2.5 km offshore. A plume 9–10 km high deposited ~ 1 × $10^8$ $m^3$ tholeiitic tephra to the northeast, a deposit known as the Medieval Tephra Layer [16, 17].

## Cordón Caulle 2011

A long-lasting eruption of Cordón Caulle, in the Puyehue-Cordón Caulle volcanic complex of Chile, began on June 4 2011. The plume reached a maximum height of ~ 12 km, and ~ 1 x $10^9$ $m^3$ of rhyolitic tephra was deposited in three phases to the east–southeast, north and east on 4–7 June. Further, less intense pulses continued until January 2012 [18].

## Campei Flegrei

The Campi Flegrei Agnano Monte Spino eruption occurred ~ 4.1 ka BP. It consisted of both hydromagmatic and magmatic activity and alternating fall and co-pyroclastic density current deposits. Trachytic ash was dispersed to the northeast, with 1.23–1.56 x $10^9$ $m^3$ of ash fallout from a 23 km high plume during phase B1 and 1.62–2.04 x $10^9$ $m^3$ of ash fallout from a 30 km plume during phase D1 [19].

The Astoni eruption consists of seven phases of hydromagmatic and magmatic activity, with Unit 6 (Astroni-6) deposited ~ 4.2 ka BP. The latter part of this unit was magmatic, producing 4.2–6.3 x $10^8$ $m^3$ of trachytic ash dispersed to the east from a plume 14 km high [19].

## Chaitén 2008

The 2008–2013 eruption of Chaitén volcano in Chile included a Subplinian explosive phase on 6 May 2008, which produced a plume 18–20 km high and dispersed 3 × $10^8$ $m^3$ of rhyolitic tephra to the northeast [20]

## El Chichón 1982

El Chichón is situated in Chiapas state, south east Mexico. The 28 March–11 April 1982 eruption consisted of three Plinian phases interspersed with smaller phreatic eruptions. The initial hydromagmatic phase lasted 5–6 hours and produced 2.9 × $10^8$ $m^3$ of trachyandesitic tephra (Layer A), dispersed to the northeast from an ash plume 17 km high. Phases B and C then produced ash flow, fall and surge deposits [21].

## Fuego 1974

The October 1974 eruption of Fuego, in Guatemala, lasted 10 days and included a Subplinian phase on 14 October. This phase lasted approximately 5 hours and produced a plume ~ 15 km high, dispersing 4 × $10^7$ $m^3$ basaltic tephra to the southwest [22].

## Ilopango ~ 1.5 ka BP

Ilopango caldera is located in the Volcanic Arc of El Salvador. The dacite—rhyolite Tierra Blanca Joven eruption occurred between 270 and 535 CE and consisted of eight phases (depositional units $A_0$ to F). Initial magma interaction with a caldera lake or shallow aquifer deposited 3.5 x $10^8$ $m^3$ of tephra westwards from a 29 km high plume (hydromagmatic Unit A). Drier conditions resulted in magmatic

Unit B, with $1.84 \times 10^9$ $m^3$ of tephra dispersed to the southwest from a 7 km plume. Units C to F were then deposited by pyroclastic flows and the final Unit G was deposited from a co-PDC plume [23].

### Pululagua 2450 BP

Pululagua forms part of the Western Andean Volcanic Front of Ecuador. The Plinian dacitic eruption of 2450 BP occurred in calm conditions and initial hydromagmatic pulses were immediately followed by a Plinian eruption with a plume height of 28–36 km. The total tephra fall volume was ~$1.1 \times 10^9$ $m^3$ and ash fall is overlain by pyroclastic flows and surges signalling the end of the eruption [24].

### Ruapehu 1996

Mount Ruapehu is situated at the southern end of the Taupo Volcanic Zone, New Zealand. The Vulcanian eruption on 17 June 1996 lasted approximately 9 hours and produced an 8.5 km high plume, bent over by a south–southwesterly wind. Initial activity the previous day had drained the small crater lake, resulting in a magmatic eruption producing $4 \times 10^6$ $m^3$ of andesitic tephra [25–27].

### Rungwe

The plume from the ~ 4 ka BP Plinian eruption of Rungwe volcano in south western Tanzania reached ~ 33 km height in calm conditions and dispersed 3.2–$5.8 \times 10^9$ $m^3$ trachytic tephra. Ash has been recovered from sediment cores in Lake Malawi, 115 km south–southeast of the volcano [28].

### Mount St Helens 1980

The 1980 eruption of Mount St Helens, in Washington state, USA, produced a 14 km high ash plume that lasted approximately 9 hours. The eruption dispersed $1.2 \times 10^9$ $m^3$ of dacitic tephra > 500 km to the east–northeast. Aggregation and fallout of fine particles resulted in a secondary thickening of the deposit approximately 325 km from source [29].

### Soufrière St Vincent 1979

The 13–26 April 1979 eruption of Soufrière on St Vincent, in the eastern Caribbean, created a new vent in a lava island formed following the 1971–72 eruption. Magma interaction with a shallow hydrothermal system resulted in a hydromagmatic eruption lasting approximately 6 minutes on 26 April, which emptied the surrounding crater lake [30]. The eruption plume rose to 7–8 km, with dispersal to the south and east. Basaltic andesite tephra covered both St Vincent and the island of Bequia, 36 km to the south [31, 32].

## Mount Spurr

The Crater Peak vent of Mount Spurr in Alaska erupted three times in 1992, with Subplinian eruptions on 27 June, 18 August, and 16–17 September. The latter two eruptions were extensively sampled and had plumes that reached the stratosphere but ash was mainly dispersed in the upper troposphere (~ 12 km high). Ash was reported up to 1200 km from source, with aggregation of fine particles leading to secondary thickening 200–300 km from source. Both eruptions were of similar size, producing a total of 1.1 x $10^8$ $m^3$ of andesitic tephra [33, 34].

## Taupo

The Plinian, 25.4 ka BP Oruanui eruption of Taupo volcano in New Zealand produced 10 depositional units from vents within Lake Huka, a paleolake located close to the present-day Lake Taupo. Rhyolitic magma interacted with water to produce ~ 4.3 x $10^{11}$ $m^3$ of fall deposit. Unit 3 was extensively sampled and consists of > 5 x $10^9$ $m^3$ tephra, including some co-PDC ash to ~ 40 km from source [35–37].

The 130 CE eruption occurred from a northeast–southwest trending fissure centred on Horomatangi Reefs in Lake Taupo. The rhyolitic eruption consisted of six phases—of which, phases 3 and 4 were hydromagmatic when water from Lake Taupo entered the vents. Phase 3 produced the 2.5 x $10^9$ $m^3$ Hatepe ash deposit, followed by a coarser pumice bed indicating a short-lived return of magmatic conditions. Phase 4 produced the 3.2 x $10^9$ $m^3$ Rotongaio ash deposit, which is found in eroded gulleys in the Hatepe ash [38, 39].

## Towada ~ 13 ka BP

The 13 ka BP caldera-forming eruption of Towada volcano, in northern Honshu, Japan, produced the hydromagmatic Hachinohe ashfall overlain with ignimbrite. In total, 3.5 x $10^9$ $m^3$ of rhyodacitic tephra was deposited in a continuous sequence of alternating beds, suggesting a fluctuating mass eruption rate. Hydromagmatic beds of fine ash with accretionary lapilli (beds HP 1, 3 and 5) alternate with magmatic pumice lapilli beds (HP 2, 4 and 6) [40].

## S2 Change in median grain size with distance from source for eruptions with samples for both phreatomagmatic and magmatic phases

Only a few eruptions (shown in Figure S1) have phreatomagmatic and magmatic phases that have both been systematically sampled for grain size analysis. For Askja 1875, sample AS82 from phreatomagmatic Phase C is held in the University of Bristol sample store (marked as 'Distal Askja phreatopl, 110 km from source'), but the median grain size for this sample is not shown in the published plot of median grain size vs distance from source [3]. We re-weighed the sample and calculated the median grain size and it provides an important distal data point, showing that the relatively constant relationship with distance in the published data seems to extend further from source.

Other eruptions with more spatially limited sampling (< 50 km from source) include Eldgja 10th century [6] and Ilopango ~ 1.5 ka BP [23], where the difference between the wet and dry phases is less clear. For Grímsvötn 2011, sampling extended to > 100 km from source [8, 41], but the small number of samples makes it difficult to identify a clear pattern.

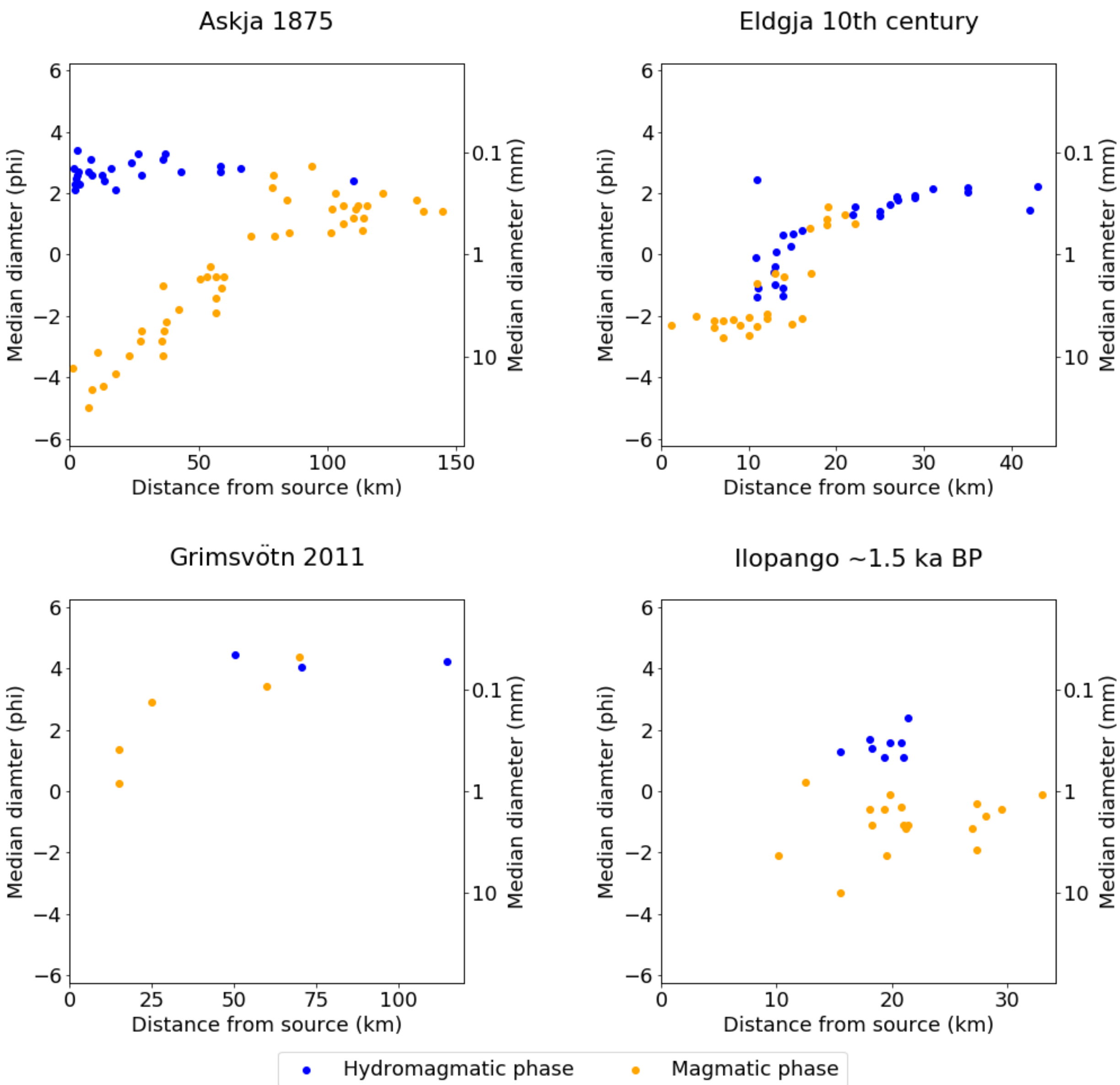


**Figure S1.** Change in median grain size with distance from source for eruptions having both phreatomagmatic and magmatic phases.

## S3 Comparison of current VAAC default particle size distribution (PSD) with equivalent values on whole-Φ and half-Φ scales

Grain size distributions are often reported in Φ units:

$\Phi = -\log_2(D/D_0)$

where $D$ = particle size (in mm), and $D_o$ = 1 mm (a reference value to make the equation internally consistent) [42].

### S3.1 Converting VAAC default micron values to Φ scale

To enable these PSDs to be input directly into NAME, we compiled and tested micron equivalents to whole-Φ and half-Φ bins

VAAC default particle size bins (Table 1) and Φ values are both uniformly distributed on a log scale, as shown in Figure S2. For the London VAAC default PSD, the log of the particle diameter is uniformly distributed within each particle size bin, and the total mass is divided evenly over the total number of particles within a bin [43]. Hence, the proportion of particles from each micron bin to be allocated to each Φ bin can be calculated by scaling, and multiplied by the relevant mass fraction to obtain the mass fraction for the new Φ bins.

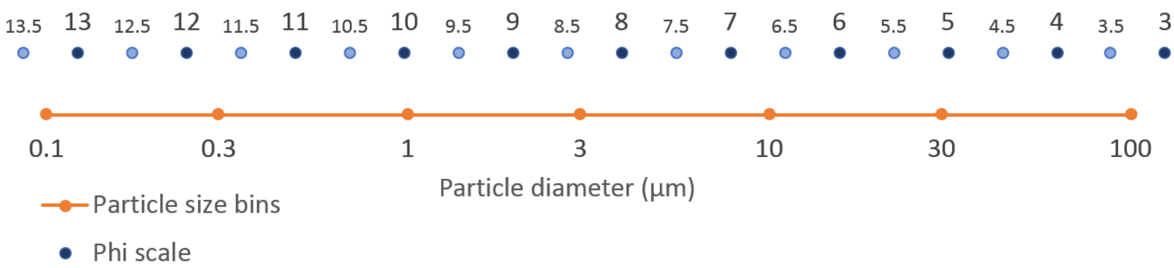


**Figure S2.** VAAC default particle size bins and Φ values plotted on log-scale Φ bins.

For each VAAC default bin, the mass of particles allocated to the equivalent Φ bins (denoted by $M_i$, $M_{i-1}$, etc.) can be defined by equation S1 for Φ bins that straddle 2 micron bins and equation S2 for Φ bins entirely within one micron bin, as shown in Figure S3a.

$$M_{i-1} = \frac{m_j(L_{j+1} - D_i)}{L_{j+1} - L_j} + \frac{m_{j+1}(D_{i-1} - L_{j+1})}{L_{j+2} - L_{j+1}} \qquad \text{(S1)}$$

$$M_{i-2} = \frac{m_{j+1}(D_{i-2} - D_{i-1})}{L_{j+2} - L_{j+1}} \qquad \text{(S2)}$$

where $D = \log_{10}(1000 \times 2^{-\Phi})$ (Φ values);

$L = \log_{10}$(micron value);

$m_j$, $m_{j+1}$, etc., are masses in the micron bins.

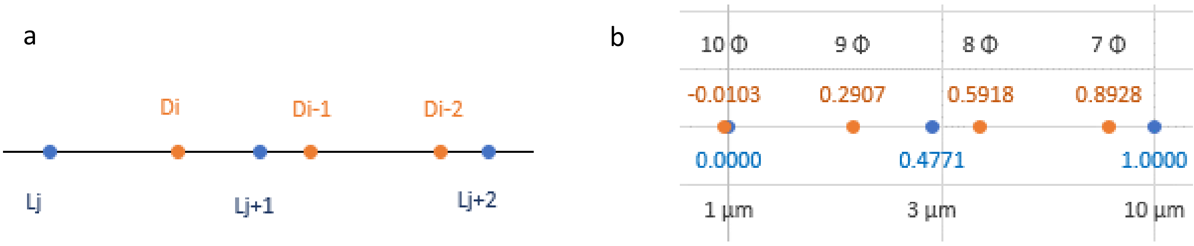


**Figure S3.** Log values of Φ and micron scales: a) general case; b) example for the 8–9 Φ bin.

An example:

The 8—9 Φ bin sits partly in the 1–3 µm bin and partly in the 3–10 µm bin, which have mass fractions of 5% and 20%, respectively.

Mass fraction for 8–9 Φ:

$$5 \times \frac{(0.4771 - 0.2907)}{(0.4771 - 0)} + 20 \times \frac{(0.5918 - 0.4771)}{(1.00 - 0.4771)} = 6.338199$$

Results for whole-Φ and half-Φ bins are shown in Tables S1 and S2, respectively.

**Table S1.** Micron equivalents of whole-Φ particle size scale and corresponding mass fractions for the VAAC default particle size distribution.

| Reported particle size (*Φ*) | Particle size range (*Φ*) | Particle size range (µm) | VAAC default mass fraction (%) |
|---|---|---|---|
| >12 | > 12 | < 0.244140625 | 0.081246 |
| 12 | 11–12 | 0.244140625–0.48828125 | 0.221047 |
| 11 | 10–11 | 0.48828125–0.9765625 | 0.287858 |
| 10 | 9–10 | 0.9765625–1.953125 | 3.056559 |
| 9 | 8–9 | 1.953125–3.90625 | 6.338199 |
| 8 | 7–8 | 3.90625–7.8125 | 11.51433 |
| 7 | 6–7 | 7.8125–15.625 | 32.53672 |
| 6 | 5–6 | 15.625–31.25 | 41.71322 |
| 5 | 4–5 | 31.25–62.5 | 2.533153 |
| 4 | 3–4 | 62.5–125 | 1.717660 |

**Table S2.** Micron equivalents of half-Φ particle size scale and corresponding mass fractions for the VAAC default particle size distribution.

| Reported particle size (Φ) | Particle size range (Φ) | Particle size range (μm) | VAAC default mass fraction (%) |
|---|---|---|---|
| > 12.5 | > 12.5 | < 0.244140625 | 0.081246 |
| 12 | 12–12.5 | 0.244140625–0.345266983 | 0.077118 |
| 11.5 | 11.5–12 | 0.345266983–0.488281250 | 0.143929 |
| 11 | 11–11.5 | 0.488281250–0.690533966 | 0.143929 |
| 10.5 | 10.5–11 | 0.690533966–0.976562500 | 0.143929 |
| 10 | 10–10.5 | 0.976562500–1.381067932 | 1.479235 |
| 9.5 | 9.5–10 | 1.381067932–1.953125 | 1.577324 |
| 9 | 9–9.5 | 1.953125–2.762135864 | 1.577324 |
| 8.5 | 8.5–9 | 2.762135864–3.90625 | 4.760874 |
| 8 | 8–8.5 | 3.90625–5.524271728 | 5.757166 |
| 7.5 | 7.5–8 | 5.524271728–7.8125 | 5.757166 |
| 7 | 7–7.5 | 7.8125–11.048543456 | 10.454179 |
| 6.5 | 6.5–7 | 11.048543456–15.625 | 22.082541 |
| 6 | 6–6.5 | 15.625–22.097086912 | 22.082541 |
| 5.5 | 5.5–6 | 22.097086912–31.25 | 19.630683 |
| 5 | 5–5.5 | 31.25–44.194173824 | 1.266577 |
| 4.5 | 4.5–5 | 44.194173824–62.5 | 1.266577 |
| 4 | 4–4.5 | 62.5–88.388347648 | 1.266577 |
| 3.5 | 3.5–4 | 88.388347648–125.0 | 0.451083 |

### S3.2 Comparison of current VAAC default PSD with equivalent values on whole-Φ and half-Φ scales

Figure S4 shows the results of NAME simulations of the Eyjafjallajökull eruption during April 2010 for different binning of PSD. Source conditions were as shown in Table 4 and times for comparison were chosen to include periods of both high and low winds, and times of stronger and weaker plumes. When comparing the result for Φ-scale bins with the current VAAC default (Table S3), the fractional bias (defined in Section S4) is very low, at < +/- 0.01 in all cases except for the half-Φ scale when wind was low and plume was high (28 April 2010 12:00 UTC). In the latter case, the plume dispersal was very limited and so even small differences between the model results are likely to have a large impact on the bias calculation.

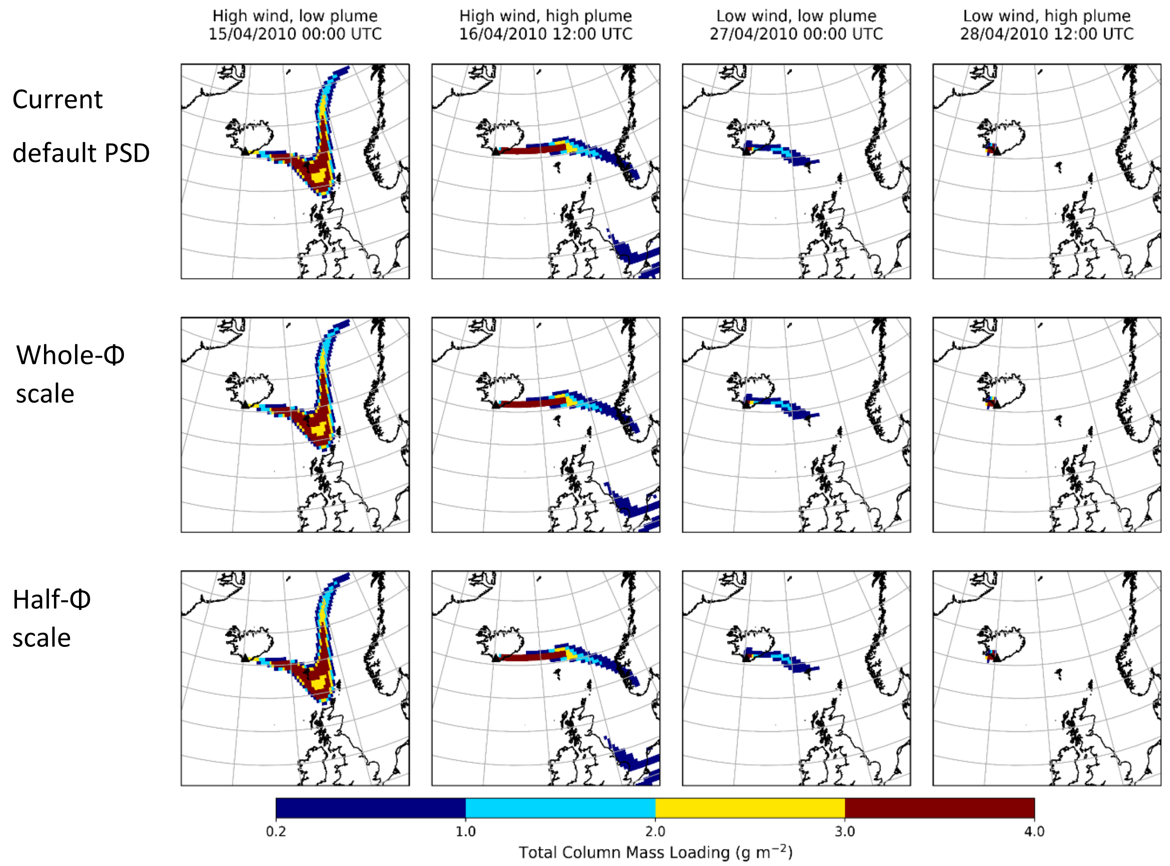


**Figure S4.** Comparison of NAME output for total column mass loading using VAAC default PSD, whole-Φ scale PSD, half-Φ scale PSD for times of high and low wind and high and low plume during the Eyjafjallajökull eruption 2010.

**Table S3.** Fractional bias of whole-Φ and half-Φ results (Figure S4) when compared with the VAAC default PSD. Fractional bias values range from -2 to +2, and positive values represent overprediction.

| | 15 April 2010 00:00 UTC | 16 April 2010 12:00 UTC | 27 April 2010 00:00 UTC | 28 April 2010 12:00 UTC |
|---|---|---|---|---|
| Whole-Φ scale | -0.002 | 0.004 | 0.001 | 0.002 |
| Half-Φ scale | -0.002 | 0.001 | -0.003 | 1.371 |

**S4 Statistical tests and residual mass loadings**

## S4.1 Residual mass loadings

Residuals represent ash mass loadings remaining when spatially and temporally paired VAAC default values have been subtracted. Positive values indicate the test loading is higher than the VAAC default value. Figures S5 and S6 show residual mass loadings for air mass loadings on 6 May 2010 12:00 UTC and 8 May 2010 00:00 UTC, respectively. Figure S7 shows the same plot for deposit mass loadings for the period 4–12 May 2010.

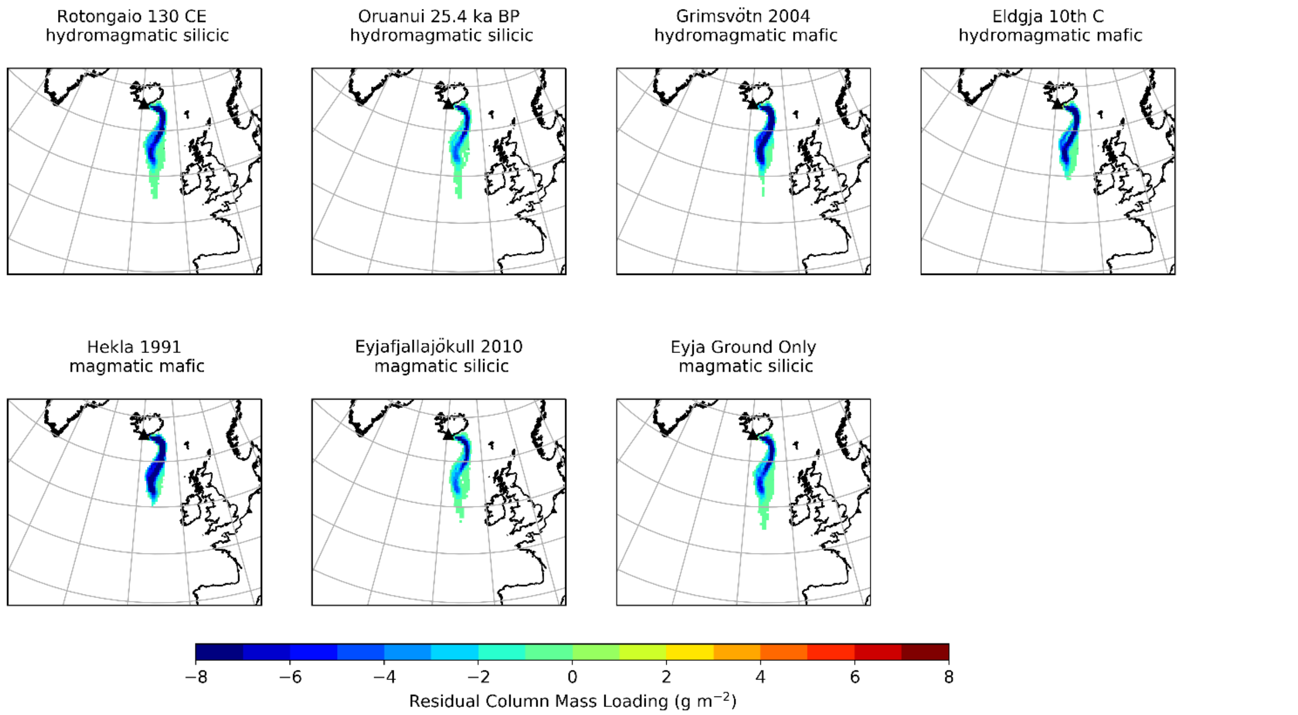


**Figure S5.** Residuals for total column mass loading for 6 May 2010 12:00 UTC after removing VAAC default PSD values.

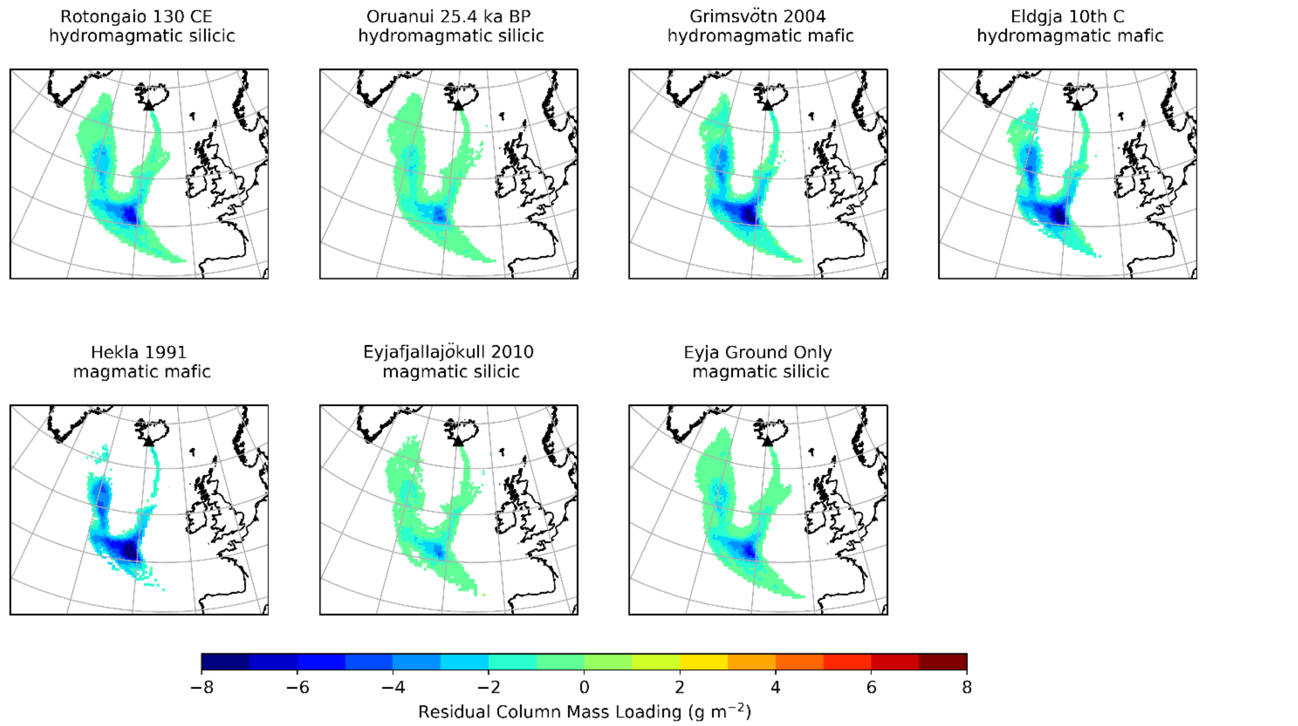

Figure S6. Residuals for total column mass loading for 8 May 2010 00:00 UTC after removing VAAC default PSD values.

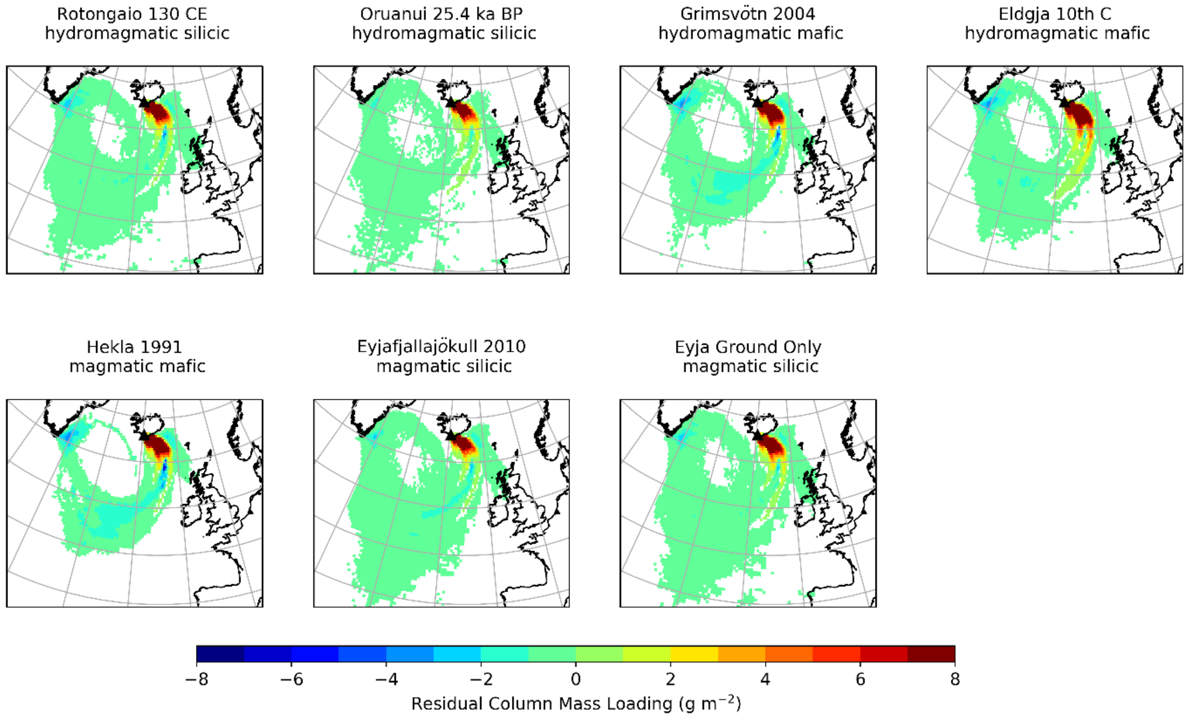


**Figure S7.** Residuals for deposit mass loadings for the period 4–12 May 2010 after removing VAAC default PSD values.

### S4.2 Statistical tests

Draxler et al. [44] summarise the range of statistical tests used to describe differences between model and measured values, and to compare simulations using different models or different input parameters for the same model. The four tests selected for this study evaluate both ash concentration and spatial extent and have been used in other studies [e.g. 45, 46]:

- Fractional bias (FB) measures systematic bias with values ranging from +2 to -2, and positive values indicating an overprediction. Results can be influenced by rare, high concentrations.
- Pearson's Correlation Coefficient (PCC) represents the linear relationship between two variables, with values of +1 and -1 indicating a positive and negative linear relationship, respectively. For dispersion models, PCC tests ash mass loadings paired in time and space and quantifies differences both the spatial extent of the plume and ash concentrations within it. PCC has been found to be sensitive to outliers.

- Figure of Merit in Space (FoM) compares the spatial extents of the plumes and is a measure of the percentage overlap of two plumes. Values range from 0 when there is no overlap to 100 for complete overlap.
- The Kolmogorov–Smirnov Parameter (KSP) represents the difference between concentration distributions, but takes no account of the spatial distribution. The KSP is the maximum difference in the cumulative distribution of unpaired concentrations and values range from 0, where distributions are identical, to 100 % for distributions with no common values.

## S4.3 Air mass loadings for 6 May 2010

### S4.3.1 Fractional Bias

| | | Test eruption | | | | | | | |
|---|---|---|---|---|---|---|---|---|---|
| | | VAAC | Rotongaio | Oruanui | Grímsvötn 2004 | Eldgja | Hekla 1991 | Eyja | Eyja Ground |
| Control eruption | VAAC | | -0.412 | -0.228 | -0.584 | -0.449 | -0.742 | - 0.218 | -0.318 |
| | Rotongaio | 0.412 | | 0.188 | -0.184 | -0.039 | -0.358 | 0.199 | 0.097 |
| | Oruanui | 0.228 | -0.188 | | -0.369 | -0.227 | -0.538 | 0.010 | -0.092 |
| | Grímsvötn 2004 | 0.584 | 0.184 | 0.369 | | 0.145 | -0.178 | 0.379 | 0.279 |
| | Eldgja | 0.449 | 0.039 | 0.227 | -0.145 | | -0.321 | 0.237 | 0.449 |
| | Hekla 1991 | 0.742 | 0.358 | 0.538 | 0.178 | 0.321 | | 0.547 | 0.452 |
| | Eyja | 0.218 | -0.199 | -0.010 | -0.379 | -0.237 | -0.547 | | -0.102 |
| | Eyja Ground | 0.318 | -0.097 | 0.092 | -0.279 | -0.449 | -0.452 | 0.102 | |

### S4.3.2 Pearson Correlation Coefficient

| | VAAC | Rotongaio | Oruanui | Grímsvötn 2004 | Eldgja | Hekla 1991 | Eyja | Eyja Ground |
|---|---|---|---|---|---|---|---|---|
| VAAC | | 0.973 | 0.992 | 0.947 | 0.965 | 0.916 | 0.992 | 0.983 |
| Rotongaio | 0.973 | | 0.995 | 0.995 | 0.997 | 0.983 | 0.994 | 0.998 |
| Oruanui | 0.992 | 0.995 | | 0.980 | 0.990 | 0.959 | 0.999 | 0.998 |
| Grímsvötn 2004 | 0.947 | 0.995 | 0.980 | | 0.996 | 0.996 | 0.979 | 0.989 |
| Eldgja | 0.965 | 0.997 | 0.990 | 0.996 | | 0.984 | 0.988 | 0.996 |
| Hekla 1991 | 0.916 | 0.983 | 0.959 | 0.996 | 0.984 | | 0.957 | 0.973 |
| Eyja | 0.992 | 0.994 | 0.999 | 0.979 | 0.988 | 0.957 | | 0.998 |
| Eyja Ground | 0.983 | 0.998 | 0.998 | 0.989 | 0.996 | 0.973 | 0.998 | |

### S4.3.3 Figure of Merit in Space

| | VAAC | Rotongaio | Oruanui | Grímsvötn 2004 | Eldgja | Hekla 1991 | Eyja | Eyja Ground |
|---|---|---|---|---|---|---|---|---|
| VAAC | | 83.17 | 89.47 | 71.36 | 71.36 | 63.32 | 90.25 | 85.93 |
| Rotongaio | 83.17 | | 92.46 | 85.80 | 85.80 | 76.13 | 91.18 | 96.21 |
| Oruanui | 89.47 | 92.46 | | 79.33 | 79.33 | 70.39 | 93.30 | 94.44 |
| Grímsvötn 2004 | 71.36 | 85.80 | 79.33 | | 91.89 | 88.73 | 78.24 | 83.04 |
| Eldgja | 71.36 | 85.80 | 79.33 | 91.89 | | 88.73 | 78.24 | 83.04 |
| Hekla 1991 | 63.32 | 76.13 | 70.39 | 88.73 | 88.73 | | 69.42 | 73.68 |
| Eyja | 90.25 | 91.18 | 93.30 | 78.24 | 78.24 | 69.42 | | 94.21 |
| Eyja Ground | 85.93 | 96.21 | 94.44 | 83.04 | 83.04 | 73.68 | 94.21 | |

### S4.3.4 Kolmogorov–Smirnov Parameter

| | VAAC | Rotongaio | Oruanui | Grímsvötn 2004 | Eldgja | Hekla 1991 | Eyja | Eyja Ground |
|---|---|---|---|---|---|---|---|---|
| VAAC | | 9.0 | 9.4 | 13.9 | 22.9 | 21.0 | 4.6 | 7.5 |
| Rotongaio | 9.0 | | 4.8 | 6.0 | 16.9 | 15.0 | 9.2 | 4.4 |
| Oruanui | 9.4 | 4.8 | | 9.0 | 13.8 | 15.5 | 10.6 | 9.4 |
| Grímsvötn 2004 | 13.9 | 6.0 | 9.0 | | 16.0 | 14.1 | 13.3 | 8.4 |
| Eldgja | 22.9 | 16.9 | 13.8 | 16.0 | | 6.6 | 23.5 | 20.5 |
| Hekla 1991 | 21.0 | 15.0 | 15.5 | 14.1 | 6.6 | | 22.4 | 21.0 |
| Eyja | 4.6 | 9.2 | 10.6 | 13.3 | 23.5 | 22.4 | | 7.4 |
| Eyja Ground | 7.5 | 4.4 | 9.4 | 8.4 | 20.5 | 21.0 | 7.4 | |

### S4.4 Air mass loadings for 8 May 2010

#### S4.4.1 Fractional Bias

| | | Test eruption | | | | | | | |
|---|---|---|---|---|---|---|---|---|---|
| | | VAAC | Rotongaio | Oruanui | Grímsvötn 2004 | Eldgja | Hekla 1991 | Eyja | Eyja Ground |
| Control eruption | VAAC | | -0.807 | -0.464 | -1.165 | -1.270 | -1.522 | -0.325 | -0.636 |
| | Rotongaio | 0.807 | | 0.378 | -0.469 | -0.622 | -1.031 | 0.516 | 0.196 |
| | Oruanui | 0.464 | -0.378 | | -0.811 | -0.945 | -1.284 | 0.145 | -0.186 |
| | Grímsvötn 2004 | 1.165 | 0.469 | 0.811 | | -0.165 | -0.640 | 0.928 | 0.649 |
| | Eldgja | 1.270 | 0.622 | 0.945 | 0.165 | | -0.488 | 1.053 | 0.793 |
| | Hekla 1991 | 1.522 | 1.031 | 1.284 | 0.640 | 0.488 | | 1.366 | 1.168 |
| | Eyja | 0.325 | -0.516 | -0.145 | -0.928 | -1.053 | -1.366 | | -0.328 |
| | Eyja Ground | 0.636 | -0.196 | 0.186 | -0.649 | -0.793 | -1.168 | 0.328 | |

#### S4.4.2 Pearson Correlation Coefficient

| | VAAC | Rotongaio | Oruanui | Grímsvötn 2004 | Eldgja | Hekla 1991 | Eyja | Eyja Ground |
|---|---|---|---|---|---|---|---|---|
| VAAC | | 0.987 | 0.995 | 0.956 | 0.905 | 0.846 | 0.990 | 0.991 |
| Rotongaio | 0.987 | | 0.993 | 0.985 | 0.948 | 0.910 | 0.984 | 0.995 |
| Oruanui | 0.995 | 0.993 | | 0.972 | 0.933 | 0.881 | 0.985 | 0.993 |
| Grímsvötn 2004 | 0.956 | 0.985 | 0.972 | | 0.965 | 0.953 | 0.962 | 0.979 |
| Eldgja | 0.905 | 0.948 | 0.933 | 0.965 | | 0.973 | 0.890 | 0.930 |
| Hekla 1991 | 0.846 | 0.910 | 0.881 | 0.953 | 0.973 | | 0.848 | 0.889 |
| Eyja | 0.990 | 0.984 | 0.985 | 0.962 | 0.890 | 0.848 | | 0.992 |
| Eyja Ground | 0.991 | 0.995 | 0.993 | 0.979 | 0.930 | 0.889 | 0.992 | |

### S4.4.3 Figure of Merit in Space

| | VAAC | Rotongaio | Oruanui | Grímsvötn 2004 | Eldgja | Hekla 1991 | Eyja | Eyja Ground |
|---|---|---|---|---|---|---|---|---|
| VAAC | | 80.18 | 89.82 | 68.79 | 58.41 | 38.68 | 89.94 | 85.32 |
| Rotongaio | 80.18 | | 88.60 | 85.57 | 72.64 | 48.18 | 86.65 | 92.99 |
| Oruanui | 89.82 | 88.60 | | 76.51 | 64.96 | 43.01 | 91.68 | 92.67 |
| Grímsvötn 2004 | 68.79 | 85.57 | 76.51 | | 79.80 | 56.22 | 74.44 | 80.63 |
| Eldgja | 58.41 | 72.64 | 64.96 | 79.80 | | 65.34 | 63.11 | 68.25 |
| Hekla 1991 | 38.68 | 48.18 | 43.01 | 56.22 | 65.34 | | 41.85 | 45.33 |
| Eyja | 89.94 | 86.65 | 91.68 | 74.44 | 63.11 | 41.85 | | 91.98 |
| Eyja Ground | 85.32 | 92.99 | 92.67 | 80.63 | 68.25 | 45.33 | 91.98 | |

### S4.4.4 Kolmogorov–Smirnov Parameter

| | VAAC | Rotongaio | Oruanui | Grímsvötn 2004 | Eldgja | Hekla 1991 | Eyja | Eyja Ground |
|---|---|---|---|---|---|---|---|---|
| VAAC | | 13.2 | 8.2 | 18.0 | 19.7 | 23.8 | 5.6 | 10.4 |
| Rotongaio | 13.2 | | 6.4 | 7.4 | 14.4 | 16.0 | 8.4 | 3.4 |
| Oruanui | 8.2 | 6.4 | | 13.0 | 15.0 | 19.7 | 8.0 | 4.3 |
| Grímsvötn 2004 | 18.0 | 7.4 | 13.0 | | 12.0 | 12.3 | 14.8 | 10.4 |
| Eldgja | 19.7 | 14.4 | 15.0 | 12.0 | | 7.2 | 21.1 | 17.0 |
| Hekla 1991 | 23.8 | 16.0 | 19.7 | 12.3 | 7.2 | | 21.3 | 18.0 |
| Eyja | 5.6 | 8.4 | 8.0 | 14.8 | 21.1 | 21.3 | | 5.7 |
| Eyja Ground | 10.4 | 3.4 | 4.3 | 10.4 | 17.0 | 18.0 | 5.7 | |

## S4.5 Deposits

### S4.5.1 Fractional Bias

| | | Test eruption | | | | | | | |
|---|---|---|---|---|---|---|---|---|---|
| | | VAAC | Rotongaio | Oruanui | Grímsvötn 2004 | Eldgja | Hekla 1991 | Eyja | Eyja Ground |
| Control eruption | VAAC | | 0.265 | 0.201 | 0.336 | 0.361 | 0.398 | 0.068 | 0.213 |
| | Rotongaio | -0.265 | | -0.064 | 0.073 | 0.098 | 0.137 | -0.198 | -0.052 |
| | Oruanui | -0.201 | 0.064 | | 0.137 | 0.162 | 0.201 | -0.134 | 0.012 |
| | Grímsvötn 2004 | -0.336 | -0.073 | -0.137 | | 0.026 | 0.065 | -0.269 | -0.125 |
| | Eldgja | -0.361 | -0.098 | -0.162 | -0.026 | | 0.039 | -0.295 | -0.150 |
| | Hekla 1991 | -0.398 | -0.137 | -0.201 | -0.065 | -0.039 | | -0.333 | -0.189 |
| | Eyja | -0.068 | 0.198 | 0.134 | 0.269 | 0.295 | 0.333 | | 0.146 |
| | Eyja Ground | -0.213 | 0.052 | -0.012 | 0.125 | 0.150 | 0.189 | -0.146 | |

### S4.5.2 Pearson Correlation Coefficient

| | VAAC | Rotongaio | Oruanui | Grímsvötn 2004 | Eldgja | Hekla 1991 | Eyja | Eyja Ground |
|---|---|---|---|---|---|---|---|---|
| VAAC | | 0.599 | 0.686 | 0.569 | 0.634 | 0.542 | 0.671 | 0.642 |
| Rotongaio | 0.599 | | 0.993 | 0.999 | 0.992 | 0.996 | 0.995 | 0.997 |
| Oruanui | 0.686 | 0.993 | | 0.988 | 0.994 | 0.980 | 0.999 | 0.998 |
| Grímsvötn 2004 | 0.569 | 0.999 | 0.988 | | 0.990 | 0.998 | 0.991 | 0.995 |
| Eldgja | 0.634 | 0.992 | 0.994 | 0.990 | | 0.980 | 0.995 | 0.998 |
| Hekla 1991 | 0.542 | 0.996 | 0.980 | 0.998 | 0.980 | | 0.983 | 0.987 |
| Eyja | 0.671 | 0.995 | 0.999 | 0.991 | 0.995 | 0.983 | | 0.999 |
| Eyja Ground | 0.642 | 0.997 | 0.998 | 0.995 | 0.998 | 0.987 | 0.999 | |

### S4.5.3 Figure of Merit in Space

| | VAAC | Rotongaio | Oruanui | Grímsvötn 2004 | Eldgja | Hekla 1991 | Eyja | Eyja Ground |
|---|---|---|---|---|---|---|---|---|
| VAAC | | 64.62 | 82.04 | 47.17 | 52.40 | 35.97 | 81.20 | 72.17 |
| Rotongaio | 64.62 | | 78.11 | 72.89 | 80.64 | 55.69 | 77.58 | 88.52 |
| Oruanui | 82.04 | 78.11 | | 57.47 | 63.83 | 43.86 | 86.60 | 86.15 |
| Grímsvötn 2004 | 47.17 | 72.89 | 57.47 | | 85.21 | 75.84 | 57.08 | 65.35 |
| Eldgja | 52.40 | 80.64 | 63.83 | 85.21 | | 68.68 | 63.17 | 72.39 |
| Hekla 1991 | 35.97 | 55.69 | 43.86 | 75.84 | 68.68 | | 43.56 | 49.87 |
| Eyja | 81.20 | 77.58 | 86.60 | 57.08 | 63.17 | 43.56 | | 86.45 |
| Eyja Ground | 72.17 | 88.52 | 86.15 | 65.35 | 72.39 | 49.87 | 86.45 | |

### S4.5.4 Kolmogorov–Smirnov Parameter

| | VAAC | Rotongaio | Oruanui | Grímsvötn 2004 | Eldgja | Hekla 1991 | Eyja | Eyja Ground |
|---|---|---|---|---|---|---|---|---|
| VAAC | | 18.9 | 9.4 | 28.9 | 30.4 | 38.5 | 12.9 | 16.0 |
| Rotongaio | 18.9 | | 9.8 | 10.2 | 14.4 | 21.4 | 11.9 | 6.0 |
| Oruanui | 9.4 | 9.8 | | 19.7 | 22.4 | 30.2 | 5.0 | 7.2 |
| Grímsvötn 2004 | 28.9 | 10.2 | 19.7 | | 7.8 | 14.0 | 20.8 | 14.6 |
| Eldgja | 30.4 | 14.4 | 22.4 | 7.8 | | 9.9 | 25.1 | 19.7 |
| Hekla 1991 | 38.5 | 21.4 | 30.2 | 14.0 | 9.9 | | 32.4 | 26.8 |
| Eyja | 12.9 | 11.9 | 5.0 | 20.8 | 25.1 | 32.4 | | 6.6 |
| Eyja Ground | 16.0 | 6.0 | 7.2 | 14.6 | 19.7 | 26.8 | 6.6 | |

### S5 References for supplementary material


1. Carey, R. J., Houghton, B. F., & Thordarson, T. (2010). Tephra dispersal and eruption dynamics of wet and dry phases of the 1875 eruption of Askja Volcano, Iceland. *Bulletin of Volcanology*, *72*(3), 259–278. doi:10.1007/s00445-009-0317-3
2. Janebo, M. H. (2016). *Historic explosive eruptions of Hekla and Askja volcanoes, Iceland: eruption dynamics and source parameters. Ph.D. Thesis*. University of Hawai'i at Manoa.
3. Sparks, R. S. J., Wilson, L., & Sigurdsson, H. (1981). The pyroclastic deposits of the 1875 eruption of Askja, Iceland. *Philosophical Transactions of the Royal Society A: Mathematical, Physical and Engineering Sciences*, *299*(1447), 241–273. doi:10.1098/rsta.1981.0023
4. Gudmundsson, M. T., Thordarson, T., Höskuldsson, Á., Larsen, G., Björnsson, H., Prata, F. J., …

Jónsdóttir, I. (2012). Ash generation and distribution from the April-May 2010 eruption of Eyjafjallajökull, Iceland. *Scientific Reports*, *2*(1), 572. doi:10.1038/srep00572

5. Liu, E. J., Cashman, K. V., Rust, A. C., & Höskuldsson, A. (2017). Contrasting mechanisms of magma fragmentation during coeval magmatic and hydromagmatic activity: the Hverfjall Fires fissure eruption, Iceland. *Bulletin of Volcanology*, *79*(10), 68. doi:10.1007/s00445-017-1150-8
6. Moreland, W. M. (2017). *Explosive activity in flood lava eruptions: a case study of the 10th century Eldgja eruption, Iceland. Ph.D. Thesis.* University of Iceland.
7. Jude-Eton, T. C., Thordarson, T., Gudmundsson, M. T., & Oddsson, B. (2012). Dynamics, stratigraphy and proximal dispersal of supraglacial tephra during the ice-confined 2004 eruption at Grímsvötn Volcano, Iceland. *Bulletin of Volcanology*, *74*(5), 1057–1082. doi:10.1007/s00445-012-0583-3
8. Olsson, J., Stipp, S. L. S., Dalby, K. N., & Gislason, S. R. (2013). Rapid release of metal salts and nutrients from the 2011 Grímsvötn, Iceland volcanic ash. *Geochimica et Cosmochimica Acta*, *123*, 134–149. doi:10.1016/J.GCA.2013.09.009
9. Stevenson, J. A., Loughlin, S. C., Font, A., Fuller, G. W., MacLeod, A., Oliver, I. W., … Dawson, I. (2013). UK monitoring and deposition of tephra from the May 2011 eruption of Grímsvötn, Iceland. *Journal of Applied Volcanology*, *2*(1), 3. doi:10.1186/2191-5040-2-3
10. Janebo, M. H., Houghton, B. F., Thordarson, T., Bonadonna, C., & Carey, R. J. (2018). Total grain-size distribution of four Subplinian–Plinian tephras from Hekla volcano, Iceland: implications for sedimentation dynamics and eruption source parameters. *Journal of Volcanology and Geothermal Research*, *357*, 25–38. doi:10.1016/j.jvolgeores.2018.04.001
11. Crosweller, H. S., Arora, B., Brown, S. K., Cottrell, E., Deligne, N. I., Guerrero, N. O., … Venzke, E. (2012). Global database on large magnitude explosive volcanic eruptions (LaMEVE). *Journal of Applied Volcanology*, *1*, article no: 4. doi:10.1186/2191-5040-1-4
12. Gudnason, J., Thordarson, T., Houghton, B. F., & Larsen, G. (2018). The 1845 Hekla eruption: grain-size characteristics of a tephra layer. *Journal of Volcanology and Geothermal Research*, *350*, 33–46. doi:10.1016/j.jvolgeores.2017.11.025
13. Gudnason, J., Thordarson, T., Houghton, B. F., & Larsen, G. (2017). The opening subplinian phase of the Hekla 1991 eruption: properties of the tephra fall deposit. *Bulletin of Volcanology*, *79*(5), article no: 34. doi:10.1007/s00445-017-1118-8
14. Höskuldsson, Á., Óskarsson, N., Pedersen, R., Grönvold, K., Vogfjörð, K., & Ólafsdóttir, R. (2007). The millennium eruption of Hekla in February 2000. *Bulletin of Volcanology*, *70*(2), 169–182. doi:10.1007/s00445-007-0128-3
15. Gjerløw, E., Höskuldsson, A., & Pedersen, R.-B. (2015). The 1732 Surtseyan eruption of Eggøya, Jan Mayen, North Atlantic: deposits, distribution, chemistry and chronology. *Bulletin of Volcanology*, *77*(2), 14. doi:10.1007/s00445-014-0895-6
16. Höskuldsson, Á., Janebo, M., Thordarson, T., Andrésdóttir, T. B., Jónsdóttir, I., Guðnason, J., … Magnúsdóttir, A. Ö. (2018). *Total grain size distribution in selected Icelandic eruptions*. Reykjavik: University of Iceland. Retrieved from https://earthice.hi.is/sites/earthice.hi.is/files/Pdf_skjol/total_grain-size_distribution_in_selected_icelandic_eruptions_01.pdf
17. Magnúsdóttir, A. Ö. (2015). *Characteristics of the CE 1226 Medieval tephra layer from the Reykjanes volcanic system. Master's Thesis.* University of Iceland. Retrieved from https://skemman.is/bitstream/1946/20359/1/MS-Agnes Ösp.pdf
18. Pistolesi, M., Cioni, R., Bonadonna, C., Elissondo, M., Baumann, V., Bertagnini, A., … Francalanci, L. (2015). Complex dynamics of small-moderate volcanic events: the example of the 2011 rhyolitic Cordón Caulle eruption, Chile. *Bulletin of Volcanology*, *77*(1), 3. doi:10.1007/s00445-014-0898-3
19. Mele, D., Costa, A., Dellino, P., Sulpizio, R., Dioguardi, F., Isaia, R., & Macedonio, G. (2020). Total grain size distribution of components of fallout deposits and implications for magma fragmentation mechanisms: examples from Campi Flegrei caldera (Italy). *Bulletin of Volcanology*, *82*(4), 1–12. doi:10.1007/s00445-020-1368-8
20. Alfano, F., Bonadonna, C., Watt, S., Connor, C., Volentik, A., & Pyle, D. M. (2016). Reconstruction of total

grain size distribution of the climactic phase of a long-lasting eruption: the example of the 2008–2013 Chaitén eruption. *Bulletin of Volcanology*, *78*(7), 46. doi:10.1007/s00445-016-1040-5

21. Varekamp, J. C., Luhr, J. F., & Prestegaard, K. L. (1984). The 1982 eruptions of El Chichón Volcano (Chiapas, Mexico): character of the eruptions, ash-fall deposits, and gasphase. *Journal of Volcanology and Geothermal Research*, *23*(1–2), 39–68. doi:10.1016/0377-0273(84)90056-8
22. Rose, W. I., Self, S., Murrow, P. J., Bonadonna, C., Durant, A. J., & Ernst, G. G. J. (2008). Nature and significance of small volume fall deposits at composite volcanoes: insights from the October 14, 1974 Fuego eruption, Guatemala. *Bulletin of Volcanology*, *70*(9), 1043–1067. doi:10.1007/s00445-007-0187-5
23. Pedrazzi, D., Suñe-Puchol, I., Aguirre-Díaz, G. J., Costa, A., Smith, V. C., Poret, M., … Gutierrez, E. (2019). The Ilopango Tierra Blanca Joven (TBJ) eruption, El Salvador: volcano-stratigraphy and physical characterization of the major Holocene event of Central America. *Journal of Volcanology and Geothermal Research*, *377*(1 June 2019), 81–102. doi:10.1016/j.jvolgeores.2019.03.006
24. Volentik, A. C. M. (2009). *Tephra transport, sedimentation and hazards. Ph.D. Thesis.* University of South Florida. Retrieved from https://scholarcommons.usf.edu/etd/71/
25. Bryan, C. ., & Sherburn, S. (1999). Seismicity associated with the 1995–1996 eruptions of Ruapehu volcano, New Zealand: narrative and insights into physical processes. *Journal of Volcanology and Geothermal Research*, *90*(1–2), 1–18. doi:10.1016/S0377-0273(99)00016-5
26. Klawonn, M., Frazer, L. N., Wolfe, C. J., Houghton, B. F., & Rosenberg, M. D. (2014). Constraining particle size-dependent plume sedimentation from the 17 June 1996 eruption of Ruapehu Volcano, New Zealand, using geophysical inversions. *Journal of Geophysical Research: Solid Earth*, *119*(3), 1749–1763. doi:10.1002/2013JB010387
27. Bonadonna, C., Phillips, J. C., & Houghton, B. F. (2005). Modeling tephra sedimentation from a Ruapehu weak plume eruption. *Journal of Geophysical Research*, *110*(B8), B08209. doi:10.1029/2004JB003515
28. Fontijn, K., Ernst, G. G. J., Bonadonna, C., Elburg, M. A., Mbede, E., & Jacobs, P. (2011). The ~4-ka Rungwe Pumice (south-western Tanzania): a wind-still Plinian eruption. *Bulletin of Volcanology*, *73*(9), 1353–1368. doi:10.1007/s00445-011-0486-8
29. Carey, S. N., & Sigurdsson, H. (1982). Influence of particle aggregation on deposition of distal tephra from the May 18, 1980, eruption of Mount St. Helens volcano. *Journal of Geophysical Research: Solid Earth*, *87*(B8), 7061–7072. doi:10.1029/JB087iB08p07061
30. Fiske, R. S., & Sigurdsson, H. (1982). Soufriere volcano, St. Vincent: observations of its 1979 eruption from the ground, aircraft, and satellites. *Science (New York, N.Y.)*, *216*(4550), 1105–6. doi:10.1126/science.216.4550.1105
31. Poret, M., Costa, A., Folch, A., & Martí, A. (2017). Modelling tephra dispersal and ash aggregation: the 26th April 1979 eruption, La Soufrière St. Vincent. *Journal of Volcanology and Geothermal Research*, *347*, 207–220. doi:10.1016/j.jvolgeores.2017.09.012
32. Brazier, S., Davis, A. N., Sigurdsson, H., & Sparks, R. S. J. (1982). Fall-out and deposition of volcanic ash during the 1979 explosive eruption of the Soufrière of St. Vincent. *Journal of Volcanology and Geothermal Research*, *14*(3–4), 335–359. doi:10.1016/0377-0273(82)90069-5
33. Durant, A. J., & Rose, W. I. (2009). Sedimentological constraints on hydrometeor-enhanced particle deposition: 1992 Eruptions of Crater Peak, Alaska. *Journal of Volcanology and Geothermal Research*, *186*(1–2), 40–59. doi:10.1016/j.jvolgeores.2009.02.004
34. McGimsey, R. G., Neal, C. A., & Riley, C. M. (2002). *Areal distribution, thickness, mass, volume, and grain size of tephra-fall deposits from the 1992 eruptions of Crater Peak Vent, Mt. Spurr Volcano, Alaska. U.S. Geological Survey Open-File Report 01-370*. Anchorage: USGS. Retrieved from https://pubs.usgs.gov/of/2001/0370/
35. Wilson, C. J. . (2001). The 26.5 ka Oruanui eruption, New Zealand: an introduction and overview. *Journal of Volcanology and Geothermal Research*, *112*(1–4), 133–174. doi:10.1016/S0377-0273(01)00239-6
36. Van Eaton, A. R., & Wilson, C. J. N. (2013). The nature, origins and distribution of ash aggregates in a large-scale wet eruption deposit: Oruanui, New Zealand. *Journal of Volcanology and Geothermal Research*, *250*, 129–154. doi:10.1016/j.jvolgeores.2012.10.016
37. Self, S. (1983). Large-scale phreatomagmatic silicic volcanism: a case study from New Zealand. *Journal of*

*Volcanology and Geothermal Research*, *17*(1–4), 433–469. doi:10.1016/0377-0273(83)90079-3

38. Smith, R. T., & Houghton, B. F. (1995). Vent migration and changing eruptive style during the 1800a Taupo eruption: new evidence from the Hatepe and Rotongaio phreatoplinian ashes. *Bulletin of Volcanology*, *57*(6), 432–439. doi:10.1007/BF00300987

39. Walker, G. P. L. (1981). Characteristics of two phreatoplinian ashes, and their water-flushed origin. *Journal of Volcanology and Geothermal Research*, *9*(4), 395–407. doi:10.1016/0377-0273(81)90046-9

40. Hayakawa, Y. (1990). Mode of eruption and deposition of the Hachinohe phreatoplinian ash from the Towada Volcano, Japan. *Geographical Reports of Tokyo Metropolitan University*, *25*, 167–182. Retrieved from https://tokyo-metro-u.repo.nii.ac.jp/?action=repository_action_common_download&item_id=2872&item_no=1&attribute_id=18&file_no=1

41. Gudmundsson, M. T., & Larsen, G. (2016). Catalogue of Icelandic volcanoes: Grímsvötn. Retrieved July 19, 2019, from http://icelandicvolcanos.is

42. Krumbein, W. C. (1936). The use of quartile measures in describing and comparing sediments. *American Journal of Science*, *32*(188), 98–111.

43. Witham, C., Hort, M., Thomson, D., Leadbetter, S. J., Devenish, B. J., Webster, H., … Kristiansen, N. (2017). *The current volcanic ash modelling set-up at the London VAAC. Met Office technical summary.* Exeter: Met Office.

44. Draxler, R. R., Arnold, D., Galmarini, S., Hort, M. C., Jones, A., Leadbetter, S. J., … Rolph, G. (2013). *Evaluation of meteorological analyses for the radionuclide dispersion and deposition from the Fukushima Daiichi nuclear power plant accident. WMO-No 1120.* Geneva: WMO. Retrieved from http://library.wmo.int/pmb_ged/wmo_1120_en.pdf

45. Beckett, F. M., Witham, C. S., Hort, M. C., Stevenson, J. A., Bonadonna, C., & Millington, S. C. (2015). Sensitivity of dispersion model forecasts of volcanic ash clouds to the physical characteristics of the particles. *Journal of Geophysical Research: Atmospheres*, *120*(22), 11,636-11,652. doi:10.1002/2015JD023609

46. Leadbetter, S. J., Hort, M. C., Jones, A. R., Webster, H. N., & Draxler, R. R. (2015). Sensitivity of the modelled deposition of Caesium-137 from the Fukushima Dai-ichi nuclear power plant to the wet deposition parameterisation in NAME. *Journal of Environmental Radioactivity*, *139*, 200–211. doi:10.1016/j.jenvrad.2014.03.018